Discovery and characterization of spontaneous mouse models of craniofacial dysmorphology

Kristina Palmer[1], **Heather Fairfield**[1], **Suhaib Borgeia**[2], **Michelle Curtain**[1], **Mohamed G. Hassan**[2], **Louise Dionne**[1], **Son Yong Karst**[1], **Harold Coombs**[1], **Laura G. Reinholdt**[1], **David E. Bergstrom**[1], **Leah Rae Donahue**[1], **Timothy C. Cox**[2,3], and **Stephen A. Murray**[1,*]

[1]The Jackson Laboratory, Bar Harbor ME 04609

[2]Seattle Children's Research Institute, Seattle WA 98101

[3]University of Washington, Department of Pediatrics (Craniofacial Medicine), Seattle WA 98195

Abstract

Craniofacial abnormalities are among the most common features of human genetic syndromes and disorders. The etiology of these conditions is often complex, influenced by both genetic context and the environment. Frequently, craniofacial abnormalities present as part of a syndrome with clear comorbid phenotypes, providing additional insight into mechanisms of the causative gene or pathway. The mouse has been a key tool in our understanding of the genetic mechanisms of craniofacial development and disease, and can provide excellent models for human craniofacial abnormalities. While powerful genetic engineering tools in the mouse have contributed significantly our understanding of craniofacial development and dysmorphology, forward genetic approaches provide an unbiased means to identify new genes and pathways. Moreover, spontaneous mutations can occur on any number of genetic backgrounds, potentially revealing critical genes that require a specific genetic context. Here we report discovery and phenotyping of 43 craniofacial mouse models, derived primarily from a screen for spontaneous mutations in production colonies at the Jackson Laboratory. We identify the causative gene for 33 lines, including novel genes in pathways not previously connected to craniofacial development, and novel alleles of known genes that present with unique phenotypes. Together with our detailed characterization, this work provides a valuable gene discovery resource for the craniofacial community, and a rich source of mouse models for further investigation.

Introduction

Of the more than 5,000 known human genetic syndromes, over 700 have craniofacial abnormalities which may include malformations such as cleft lip and palate, abnormal skull, face, or jaw morphology, missing teeth, and eye and ear abnormalities. (Gorlin and Stefan,

*Corresponding Author: The Jackson Laboratory, 600 Main St., Bar Harbor, Maine 04609 USA, 207-288-6857, FAX 207-288-6149, steve.murray@jax.org.

1990). Genetic or environmental factors or an interaction between the two contribute to these disorders. Craniofacial abnormalities can have significant impact on sensory organs, breathing, swallowing, and potentially devastating psychological and social consequences. Repair often requires extensive surgical intervention, so the development of animal models for these disorders is of great importance to the scientific community.

Identification and an understanding of the genes controlling craniofacial development are critical to elucidating genetic etiology of craniofacial abnormalities. Mouse models are outstanding genetic models for the analysis and understanding of inherited human disease. They offer many of the advantages of simpler model organisms, including a short reproductive cycle and simple husbandry requirements, but as mammals more accurately recapitulate many human conditions. The bones of the mouse skull are remarkably similar to the homologous bones in the human skull. Moreover, craniofacial disorders are shared between species. Together with a rich array of tools and resources for both genome manipulation and complex genetics, the mouse provides an ideal model for understanding the genetic causes of craniofacial dysmorphology.

Much of our current understanding of craniofacial biology in the mouse has been driven by reverse genetic tools and resources available for the mouse, including knockout alleles, cre driver alleles and loxP-flanked target genes, and now genome editing platforms that facilitate rapid modification of precise alleles, including putative human causal variants. While incredibly informative and productive, such hypothesis-driven approaches are necessarily biased by preliminary data implicating a given gene or pathway. Forward genetic, or phenotype-driven, screens provide an unbiased means to identify novel genes and pathways underlying a specific phenotype or condition. Spontaneous mutations provide a further level of unbiased discovery, as new deviants can arise on any genetic background and thus reveal a phenotype that would have been missed on a limited number of inbred backgrounds. Until the advent of high-throughput sequencing (HTS) approaches, identification of the causative gene was the major bottleneck in spontaneous and ENU-induced mutant discovery programs. Recent work (Fairfield et al., 2011a; Fairfield et al., 2015), has clearly demonstrated that exome and whole-genome sequencing can now be applied to efficiently identify potential causative variants. These advances have greatly enhanced our ability to identify numerous new spontaneous models of craniofacial dysmorphology that add to our understanding of the genes and pathways that are critical for craniofacial development.

Inherited craniofacial disorders in both humans and in mice seldom occur in isolation. They are typically seen as part of a broader syndrome of clinical and phenotypic manifestations resulting from disruption of a specific gene and pathway. Most studies, however, focus deeply on a specific phenotype that is either primary, or falls within the expertise of the investigator. These missing data, however, can be critical to a full understanding of gene function and the pathogenesis of the condition being modeled. Recognizing this gap, recent efforts, such as the NIH-funded KOMP2 program and the International Mouse Phenotyping Consortium, have emphasized broad-based, standardized phenotyping as a means to supplement deep, hypothesis-driven characterization. Indeed, results from some of these programs have shown that not only are phenotypes frequently missed (Ayadi et al., 2012;

Fuchs et al., 2012), but that pleiotropy is more common than not, highlighting the need for breadth in characterization to accompany depth.

Here, we present the Craniofacial Mutant Resource, our long-standing effort to take advantage of the large mouse breeding colonies at the Jackson Laboratory, the scale of which leads to the frequent appearance of spontaneous mutants to provide mouse models of craniofacial dysmorphology. We describe the identification and characterization of 43 models, including 33 for which the causative gene has been discovered. In addition to characterization of the craniofacial phenotypes, we demonstrate that a majority of these lines also display phenotypic abnormalities in a number of areas, particularly in growth and body composition. These models include genes for which all existing models are lethal, novel genes not previously associated with craniofacial development or disease, and genes where the specific genetic background reveals a disease model masked by typically used inbred strains. All of the mice are publically available from the resource, and our ongoing screen routinely identifies new models that will contribute to the collection. Together, this resource provides a unique and rich source of discovery tools for craniofacial biology.

Results/Discussion

The Craniofacial Mouse Resource acquires mice primarily through our internal "deviant search" program, mice with visibly apparent phenotypic deviations from distribution colonies and from individual, private research colonies. Animals with a range of craniofacial abnormalities, including deviations in head shape, dentition, ear shape and/or position and structural eye defects are selected for further investigation. Additional deviants are identified in individual research colonies. A significant proportion of murine craniofacial dysmorphologies are not heritable or frequency display variable penetrance and/or expressivity. Analysis of each spontaneous line begins with mating the affected animal to an unrelated mouse of the same strain to establish heritability and mode of inheritance. To simplify genetic mapping and phenotypic characterization, we only pursue mutations with greater than 10-20% penetrance of the primary phenotype. Of the 470 strains received to date, 286 displayed heritable phenotypes, 73 of which were ultimately discarded due to low penetrance. From this set, we pursued characterization and gene discovery for 78 individual lines, of which 43 are complete and described in this study. Lines described here and future lines identified in our screen are posted at faces.jax.org, and all data are deposited in Mouse Genome Informatics (informatics.jax.org) on a regular basis.

A summary of the 43 models identified and characterized by the resource is shown in Figure 1A. These comprise a range of craniofacial and easily discernable comorbid phenotypes, including 22 with abnormal nose length/shape, 9 with abnormal head shape, 11 ear shape/ position mutants and 5 models with defective tooth development. In addition, these were frequently comorbid with eye, hair, limb and body shape abnormalities, and several mutants were infertile or displayed reduced fertility. Both dominant/semi-dominant (19) and recessive (24) mutants were recovered. A complete, detailed description of 17 of these models, including phenotype data, gene discovery details and mutation details, is included in the Supplementary files 1-17.

Craniofacial abnormalities were assessed using either alizarin red skeletal preparations and a standard set of landmark-based measurements (Richtsmeier et al., 2000) or, for mutant characterized more recently, whole head microCT to capture high-resolution three-dimensional datasets. Overall, as expected, skull measurements displayed a high hit rate, with skull length abnormalities noted in nearly 80% of mutants (Figure 1B). The high hit rate is expected given the lines were identified as having overt craniofacial appearance, particularly short noses. While significant differences in all dimensions are noted (length, height, width) in our mutant collection, skull width anomalies were less common than length or height. It is unclear if this difference is simply due to the snout phenotypes being more readily discernible to the naked eye.

A key component of our pipeline is identification of the causative mutation by whole exome or whole genome sequencing. Establishment of linkage to a chromosome or sub-chromosomal interval adds significant power to mutation discovery because it reduces the field of candidate variants and ultimately, the validation burden. Because the penetrance of craniofacial phenotypes is highly sensitive to inbred strain background, linkage crosses were previously initiated with more than one inbred strain, including A/J, C3H/HeJ, and Balb/cByJ. However, new resources of whole genome sequencing data for inbred strains have provided significantly large SNP datasets from closely related inbred strains (Keane et al., 2011). Taking advantage of these data resources, we developed a new SNP panel that allows us to utilize C57BL/6NJ as a mapping strain for mutations arising on the closely related C57BL/6J strain. This mapping cross allows us to test linkage while minimizing the confounding effects of strain background. Using this approach, we established linkage for all but one of our lines (*Rdns*) using 10-12 affected F2 (recessive) or backcross (dominant) animals and controls.

Once linkage is established, we employ multiple strategies to identify the causative gene. Since remutations occur frequently, new recessive mutants that closely resemble an existing line that are readily available on the shelf are crossed to test for allelism. This has proven successful for alleles of *Bmp5 (cfe-se7J and 8J)* and *Prkra* (*lear-2J*). In some cases, prior to the routine implementation of HTS, strong candidates are identified within an interval and screened via targeted PCR amplicon sequencing. We used this approach to identify alleles of *Alx4* (*lst-2J*) and *Pfas* (*Sofa-3J*), among others. A majority of our mutant lines enter a standardized HTS exome pipeline to identify putative causative mutations (Fairfield et al., 2011b; Fairfield et al., 2015). This has proven very successful, and more than half (18) of our 33 new mutant genes were identified using this approach (Figure 1C). For a number of mutants, exome sequencing failed to identify viable candidate mutations, despite sufficient depth and coverage (for example, *sws*, *sbse*, *din*, *frg*, *snol* and *He*). There are a number of explanations for this outcome. For example mutations outside our current exome design (either non-coding or newly annotated genes) or structural mutations (e.g. duplications, inversions) can escape detection by exome pipelines. Standard exome pipelines are optimized for single nucleotide variants (SNVs) and small insertions/deletions (INDELs) and often fail to detect larger (> 50 bp) structural variants. For example, our exome pipeline failed to detect an inversion in *Tnsf11* that we later discovered through manual analysis of alignment data (see below, Figure 5).

Given the clear pleiotropy evident from simple inspection of the individual lines, we subjected mutants to a series of phenotypic assessments to expand upon and quantify these observations (Figure 2A; all data summarized and available in Supplemental Tables 1 and 2). These tests included measures of body growth, body composition, hearing, vision, skeletal structure and histopathology. Cohort size and phenotying pipeline structure were designed to minimize the number of mice required while maintaining statistical power to identify differences between groups. Mice were characterized over an 8 week period (ages 4-12 weeks) to capture post-wean growth dynamics and typical adult physiology. As shown in Figure 2B, the majority (over 80%) of mutant lines characterized showed growth abnormalities versus (littermate) controls. Consistent with this finding, body composition measures such as lean body mass, total mass and bone mineral density (BMD) were very commonly affected in mutant lines (Figure 2C). Our histopathogical screen identified comorbid lesions in over 50% of the mutants, and deficits in hearing and vision were observed in a significant number of lines. Together, these data indicate that a majority of mutant lines originally identified on the basis of their craniofacial characteristics also show additional significant comorbid phenotypes, illustrating the pleiotropic nature of the underlying genes.

Bbfc – A novel allele in *Sox9* causative of craniofacial abnormalities

Bbfc ("Babyface") was as discovered in a C57BL/6J ENU colony in 2010. This novel dominant mutation of *Sox9* results in a shortened nose phenotype but no other obvious abnormalities. For linkage analysis, a backcross to C57BL/6NJ was performed. A mapping panel of 100 N:J substrain SNPs indicated a strong linkage to 11-114979024-S with an estimated LOD (score of 9.4308 (significance is LOD   3) and 37 of 38 animals were concordant with this marker. Whole exome sequencing (Fairfield et al., 2015) revealed a single mismatch allele of C to T on chromosome 11: 112,782,845 on (GRCm38/mm10). The SNV, located in exon one of SRY-box containing 9 (*Sox9*), is predicted to result in the missense mutation T87M (Figure 3A). We confirmed the presence of the mutation in 10 tested short nosed mice, as well as noting it in two unaffected animals, suggesting the gene is causative but the phenotype is incompletely penetrant.

MicroCT scans revealed reduced overall skull length, reduced nose length and reduced upper jaw length (Figure 3C-F), confirmed by caliper measurements of alizarin prepped skulls (Figure 3G-I). The skull height to width ratios were reduced in mutants, while the height to length ratio was increased, consistent with the overall short, domed appearance of the head. Male mutant mice were significantly smaller overall versus controls (Figure 3L), and males showed significantly lower total body fat (Figure 3M) and percentage body fat (Figure 3N). Notably, females were not significantly different for any of these measures, suggesting a high degree of sexual dimorphism. Sox9 is essential for sex determination and for the development of testes. However, no intersex or putatively sex-reversed mice were noted, and although mice were not genotyped for the Y chromosome, sex ratios are normal at birth and males are fertile. No other abnormalities in hearing, vision or pathology were noted.

Prior null alleles of *Sox9* are haploinsufficient and display perinatal lethality with cleft palate, hypoplasia and defects in numerous skeletal structures, as well as premature bone mineralization((Bi et al., 1999). Conditional knockout mutations using bone-specific cre driver lines similarly show skeletal and craniofacial abnormalities. (Akiyama et al., 2002; Bi et al., 2001; Kist et al., 2002; Seymour et al., 2008). In humans, *SOX9* mutations in humans causes Campomelic Dysplasia (OMIM: 114290), a syndrome that is characterized by defects in skeletal development and distinctive craniofacial abnormalities such as a flat face and hypertelorism. Affected individuals also show sex reversal, gonad dysplasia and/or abnormal genitalia. Unlike the null mouse alleles, human mutations are not lethal in the perinatal period, including nonsense mutations. Given the haploinsufficient lethality, existing models of null alleles are difficult to work with and must be bred from chimeras generated from ES cell injections or conditional alleles bred to a deleter cre line. Our model, though clearly hypomorphic, offers the potential to study the craniofacial abnormalities in isolation and could model less severe alleles that occur in the human population.

Pfas[Sofa]: Allelic series of a novel gene in craniofacial development

Sofa ("short face") was discovered in a production colony of C57BL/6J-Apc[Min]/J mice in 2000. Mutants are dominant and characterized by a short, upturned nose and incompletely penetrant white belly spotting. Linkage crosses identified a critical interval on Chr 11, and subsequent exome sequencing revealed a 15bp deletion in exon 7 of the phosphoribosylformylglycinamidine synthase gene *Pfas* (Figure 4A,B,I). (Fairfield et al., 2011b) Also known as phosphoribosylformylglycinamide amidotransferase (*FGARAT*), this gene encodes the fourth component of a 10-enzyme, 6-gene *de novo* purine biosynthesis pathway that converts phosphoribosyl pyrophosphate to inosine monophosphate, which is then converted to guanine or adenine. Although it is not immediately obvious why mutation of this gene would result in craniofacial abnormalities, the face is one of the most highly proliferative tissues during the fetal and early postnatal period, especially the elongated snout of the mouse, and so this may simply reflect the impact of reduced purine availability on the rate of cell proliferation. However, accumulating evidence also supports a role for purinergic signaling in bone, cartilage and muscle (Orriss, 2015). And given the discovery of an additional five independent alleles showing essentially identical phenotypes (Figure 4A, B; full descriptions in Supplemental File 16), further investigation of the role of this gene and pathway in craniofacial development seems warranted. Notably, this allelic set includes a range of genetic lesions, such as an in frame small deletion (*Pfas*[Sofa] described above), a splice acceptor mutation at the 3′ end of intron 6 predicted to result in an in frame deletion of exon 7 (B6(Cg)-*Pfas*[Sofa-2J]/GrsrJ), INDEL-mediated frame shift mutations (B6(129S7)-*Pfas*[Sofa-3J]/GrsrJ and B6.129S1- *Pfas*[Sofa-5J]/GrsrJ) and missense mutations (C57BL/6J-*Pfas*[Sofa-4J]/GrsrJ and C57BL/6J-*Pfas*[Sofa-6J]/GrsrJ). Notably, all of the *Pfas* alleles have arisen on a C57BL/6J background, which is consistent with a decrease or loss of phenotype when outcrossed to different genetic backgrounds. Because our mutant *Pfas* alleles are dominant, we asked whether we could identify a homozygous phenotype in the *Sofa* allele. Timed matings and dissections at E12.5, E9.5, and E7.5 identified no homozygous embryos, suggesting an early lethal phenotype consistent with its central position in a fundamental biosynthetic pathway.

Three-dimensional surface rendering of microCT images reveals significant defects in skull length and shape, and significant fusions of the frontal, inter frontal and nasal bones are observed in most mutants (Figure 4B). In addition, occasional individuals show minor synostosis of the coronal suture (*Sofa-4J* in Figure 4B). While there is variation in the severity of the phenotype for all lines, all the severely affected mice have premature ossification of one (or more) cranial base synchondroses. Numerous mutants also have significantly receded alveolar bone. Caliper measurements of skeletal preparations showed differences in most measures, with some degree of sexual dimorphism (Figure 4C, D; Supplementary table 2). This includes both total skull length and nose length, and inner canthal distance (Supplemental Table 2). Skull to nose length ratio, skull height to length ratio, skull length to width ratio and inner canthal distance differed between genotypes within both sexes (Supplemental Table 2). *Sofa* mutants also showed differences in most body composition measures, including whole body mass (Figure 4E), lean body content, whole body fat content, body fat percentage, BMD and BMC (Supplemental Table 2). *Sofa* mutants showed a range of eye defects, including microphthalmia and anophthalmia, cataracts, and eye infections, all with variable penetrance.

While no other mouse mutation has been described for any of the components of the pathway, zebrafish mutants in *gart* and *paics* display transient ocular and pigmentation defects, consistent with the variable belly spotting seen in all *Sofa* alleles (i.e. mild neural crest deficiency). Human mutations have been described in *ADSL* and *ATIC*, leading to accumulation of intermediates and adenylosuccinase deficiency (OMIM:103050) and ASIC-ribosuria (OMIM: 608688), respectively, which are characterized by neurological deficits, epilepsy, and in the case of *ADSL* mutation, motor deficits.

Tnfsf11^gum, a spontaneous inversion allele resulting in osteopetrosis and failed tooth eruption

Two mutant females and one mutant male were found in a colony of STOCK Tg(Myh6-cre)1Jmk/J at the Jackson Laboratory in 2013 that displayed a primary defect in a failure of tooth eruption and clear abnormalities in body size and head shape. While males are subfertile, females have litters but pups fail to thrive and die. Some mutants also develop facial abscesses. The original male was bred to a C57BL6/J female and the two original females were bred to C57BL6/J males via ovarian transfer. Subsequent matings proved the mutation is recessive.

Prior to the initiation of linkage crosses, one homozygous and one heterozygous animal were submitted for exome sequencing. Of all high, moderate, and modifier variants identified, three were unique to this strain with allele frequency of 1.0 in the homozygote and 0.5 in the heterozygote. All variants failed to validate upon Sanger sequencing of independent affected animals. A subsequent mapping cross established linkage to Chromosome 14. While no viable candidate mutations found with our standard exome pipeline, a strong candidate gene, *Tnfsf11* (RANKL), was suggested by its knockout phenotype including osteopetrosis and failure of tooth eruption (Kong et al., 1999). Manual read pair analysis of the alignment data using Integrated Genomics Viewer (IGV) (Robinson et al., 2011) revealed read mapping patterns typical of an inversion (Keane et al., 2014)

(Figure 5A). The data revealed an approximate 4.7 kb inversion including exons 3 and 4, which was confirmed by PCR and Sanger sequencing over the inversion breakpoints. In addition to small size and a failure of tooth eruption (Figure 5B,C), mutant skulls are severely affected (Figure 5E versus D), displaying highly thickened bone overall with obvious high levels of ossification in the hyoid and zygomatic arches. There are no maxillary-premaxillary sutures, the angle and condyle of the mandible is misshapen, and the anterior part of the mandible is hypoplastic. Molars are present, but unerupted, and mutants have what appears to be an additional tooth arising in or around the mandibular foramina (Figure 5F).

Consistent with the thickened skull bones, X-rays revealed dense bones that completely occlude the medullary cavity of the long bones (Figure 5G) and display increased density in most other bones in the skeleton (Figure 5I, K). These features are consistent with an osteopetrotic phenotype and are similar to the reported phenotype of knockout alleles of *Tnfsf11* (Kong et al., 1999). Body weight and tail length measurements were recorded at 4, 6, 8 and 12 weeks of age on the same cohort of mice. The body weight curves were statistically different between genotypes, and sexes (Figure 5M), and tail length curves were different between genotypes (Supplemental Table 2). As expected, mutants displayed increased whole body bone mineral density (Figure 5N), increased whole body bone mineral content (Figure 5M), but consistent with their small size, displayed significantly less lean mass (Figure 5O).

A pathology screen confirmed that all mutants had osteopetrosis however and four of the six mutants showed signs of muscular dystrophy such as small muscle fibers (two showed signs only in the head), fiber degeneration and regeneration. One had apparently incidental abscesses below the skin, though it should be noted that many mutants develop abscesses on their faces. An overabundance of medullary bone made the medullary cavity very solid and therefore less marrow was present.

While the inversion identified in this model presented specific challenges to gene discovery, the phenotype is similar to other osteopetrotic models in that it has reduced fertility, its teeth fail to erupt, and it is visibly smaller in body size. However, we also identified what appears to be an ectopic tooth in the mandibular diastema region (specifically in the vicinity of the mandibular foramina) that has not been reported in other models. Other osteopetrotic mutants are anemic because the medullary cavity is completely solid and hence they have no bone marrow. Other alleles of *Tnfsf11* display a failure to lactate consistent with the 100% postnatal death observed in our colony of pups from homozygous females.

Prkra^lear5J, a new remutation with emergent disease phenotypes

A new deviant was identified on the BTBR T[+] Itpr3[tf]/J genetic background, which results in a small body size, small ears, kinked tails, progressive paralysis or dystonia, hearing loss, and mortality. Inheritance was determined to be recessive and analyzed directly by whole exome HTS in a pilot to determine whether direct sequencing of multiple individuals in a pedigree could replace linkage crosses, which are expensive and time consuming. Five animals from a single pedigree, including two heterozygous parents, two affected homozygous pups and one unknown but unaffected pup were sequenced using our standard

protocol. Subsequent analysis, confirmed by Sanger sequencing, revealed a two base pair insertion/deletion mutation in the *Prkra* gene on Chromosome 2 at base pair 76,636,870. This G to GT frameshift is predicted to introduce seven novel amino acids prior to a premature stop codon (Figure 6A).

This is the fifth *lear* ("little ear") allele of *Prkra* identified at The Jackson Laboratory, and thus designated *lear-5J*. Consistent with the other known *Prkra* alleles, homozygous mice have small body sizes and small ears (Figure 6B) in addition to hearing loss, and are infertile; consistent with other known *Prkra* mutations. In contrast to other *Prkra^lear* alleles, however, these mice have kinked tails and show ascending dystonia or paralysis, which begins at two weeks of age and continues until death at about three weeks of age. No mutants have survived until breeding age. Pathology screens on three mutant females, six mutant males, and two wild types of each sex at three weeks of age revealed an anomaly in mutants hitherto undescribed in other *Prkra* mutants. It was noted that that some neurons in the dorsal root ganglia and in the trigeminal ganglion of the head were apoptotic or necrotic (Figure 6G,H), consistent with the putative neurodegenerative phenotype.

Skulls of *Prkra* were dramatically shorter and malformed (Figure 6C,E), including an open foramen. In addition to size and shape, skulls displayed reduced bone mineral content (Figure 6M). As described above, mice are much smaller (Figure 6I-K) and, as with all *lear* alleles, have dramatically smaller ear pinna (Figure 6L). No abnormalities were identified in X-rays of two three-week-old mutants. Normal bone structure of the kinked tail, which relaxes significantly after death, suggests that this phenotype be the result of dystonia or paralysis rather than abnormal bone structure. Some mutants also have "gnarled" or bent wrists with similarly normal bone structure.

Additional basic neurological testing was conducted on two mutant and two wild type animals at three weeks of age. Both animals were capable of directing their own movements. Wild type controls reacted via withdrawal to hind paw pinches, had strong grasping reflexes in the fore and hind paws, and appeared to have normal gaits. Both mutants had an elongated step/push gait with the hind limbs. One mutant had no grasping reflex with the hind paws but could grip with the forepaws. The other, which had gnarled wrists, had a weak grasping reflex with the forepaws and no grasping reflex with the hind paws. The first mutant reacted to a hind paw pinch only with the left hind paw and the second did not react with either paw

PRKRA has been identified in humans as the causative gene for Dystonia 16 (OMIM: DYT16 (6129067)). Patients with this condition display early onset and progressive limb dystonia resulting in abnormal gait, torticollis, and orofacial dystonia and grimacing (Camargos et al., 2008; Seibler et al., 2008; Zech et al., 2014). This is the first report of a mouse model of this particular syndrome, as prior alleles of *Prkra* in mice have not shown any of the neuromuscular phenotypes apparent in *Prkra^lear5J*. Notably, this allele arose on an unusual (BTBR) genetic background, highlighting the value of an unbiased screen that includes a variety of genetic contexts. Interestingly, human patients with *PRKRA* mutations are not reported to have craniofacial abnormalities, ear morphology defects, or hearing loss, either suggesting a role for genetic modifiers in presentation of the phenotype and proper

modeling of the human condition or a specific co-opted function in the development of the mouse pinna.

Here we describe a resource that identifies, characterizes and distributes mouse models with clinical craniofacial abnormalities. Like human patients, these models are viable and harbor a wide array of comorbid phenotypes that are observed in craniofacial syndromes. The addition of phenotyping tests to capture these phenotypes adds depth to the value of the models, and sheds new light on the pleiotropic nature of many of the underlying genes. With the expansion of additional high-throughput phenotyping capacity supported by the KOMP2 program, we plan to apply this systematic phenotyping approach to new mutants in the resource.

As most of our mutants are spontaneous, the models have several unique characteristics versus standard constitutive of conditional knockout models. First, hypomorphic point mutations can reveal phenotypes masked by early lethality or other severe phenotypes, as seen in the case of $Sox9^{Bbfc}$. Indeed a majority of the mutations discovered thus far have been missense mutations, which frequently retain some gene function. Second, forward genetic screens are unbiased and have to potential to uncover truly novel genes that contribute to a phenotype, such as our allelic series of *Pfas,* thus expanding understanding of the genes and pathways that contribute to craniofacial development and dysmorphology. Third, structural mutations, which are common in human conditions, are frequently identified in our screen as well. The inversion of *Tnfsf11* is one of the first inversions to be detected by HTS in the mouse. While there are still challenges around computational identification of structural mutations, these tools are improving and our spontaneous "raw material" will prove a useful testing ground for these tools. Finally, by pulling spontaneous mutants from the breeding colonies at JAX, mutations can (and do) arise on any genetic background. This provides a unique opportunity to examine gene function in genetic contexts beyond a small handful of mouse strains. While the first four alleles of *Prkra* displayed a similar spectrum of ear phenotypes, in a BTBR T$^+$ Itpr3^{tf}/J genetic context, the mutation presented with a variety of phenotypes that recapitulate conditions resulting from human mutations in *PRKRA*. As a living collection that continues to identify and characterize mutants, it will continue to deliver a unique assortment of important craniofacial models to the scientific community.

Methods

Animals and husbandry

Mice were housed in 51 square inch polycarbonate boxes on sterilized Northern White Pine bedding under 14:10 hour light:dark cycles. Autoclaved NIH 31 (6% fat diet, Ca:P of 1.15:0.85, 19% protein, vitamin and mineral fortified; Purina Mills International, Richmond, IN) grain and water acidified with HCl to achieve a pH of 2.8-3.2 were freely available. Mouse colony maintenance and use is reviewed and approved by The Jackson Laboratory Institutional Animal Care and Use Committee and is in accordance with The National Institutes of Health guidelines for the care and use of animals in research.

Genetic mapping

Linkage crosses are established by outcrossing to a strain (empirically determined) that retains phenotypic penetrance. 10-12 affected individuals are typed genome wide using microsatellite markers or SNP markers. Linkage analysis and recombination frequencies are calculated via the Map Manager computer program (Manly, 2001). For HTS, single chromosome resolution is sufficient to proceed, although we typically achieve intervals of 20-50Mb.

Exome Sequencing

Exome sequencing was performed as described (Fairfield et al., 2015). Briefly, Illumina paired end (PE) libraries (2×76 or 2×100) were prepared from genomic DNA and liquid phase sequence capture were performed as previously described using the Roche NimbleGen SeqCap EX Mouse Exome Design (110624_MM9_Exome L2R_D02_EZ_HX1, #99990-42611) (Fairfield et al., 2011b). Enriched libraries were sequenced on the Illumina GAIIx or the Illumina HiSeq (Illumina, San Diego, CA). Data analysis was performed as previously described (Fairfield et al. 2015). Briefly, sequencing reads were subjected to quality control and mapped to the mouse genome (GRCm38, mm10) using BWA. Duplicates were removed (Picard MarkDuplicates module, http:picard.sourceforge.net) and The Genome Analysis Tool Kit (GATK) v2.2-16 modules were used for alignment preprocessing and variant calling. Variants were annotated by SnpEff v2.0.5 and ANNOVAR. GATK VariantAnnotator reported those of highest impact. Variant data and annotated VCF files are available through the JAX MMR database (https://mmrdb.jax.org/mmr/). High priority was given to protein coding or splice variants within mapped regions, as well as unique variants that were not found in other exome data sets or in variant data from the Sanger Mouse Genomes Project (www.sanger.ac.uk/resources/mouse/genomes). Putative causative variants were validated by re-sequencing and co-segregation analysis in relevant pedigrees.

Skull Preparation

Skulls of 6 male and 6 female mutants and controls are collected at 12 weeks of age, prepared by incomplete maceration in potassium hydroxide, stained with alizarin red, and stored in undiluted glycerin (Green, 1952). During the collection process, right ear pinnae are measured with digital hand calipers (Stoelting, Wood Dale, IL, USA).

Hand Caliper Skull Measurements

Seven measurements taken with hand held digital calipers are used routinely to define skull morphology. These measures have a high degree of accuracy and precision in our hands and are able to discriminate differences between mutant and control skull characteristics (Richtsmeier et al., 2000).

MicroCT

JAX—Skulls for microCT scanning were collected from mutant and control mice and frozen at -20C until they imaged. Skulls were then thawed and placed in 20ml plastic scintillation vials and the caps were sealed. The sealed vials were then mounted to a brass

holder with warmed paraffin and scanned with microCT scanned with a Skyscan 1172 microCT scanner (Bruker BioSpin Corporation, 15 Fortune Drive, Billerica, MA). Images were reconstructed using NRecon software (Bruker BioSpin Corporation, 15 Fortune Drive, Billerica, MA) and surface rendered with Imaris software (Bitplane AG, Zurich Switzerland).

UW—Animals were imaged at the Small ANimal Tomographic Analysis (SANTA) Facility at Seattle Children's Research Institute using a Skyscan model 1076 micro-computed tomograph (microCT) (Kontich, Belgium). Scans were done at an isotropic resolution of 34.42 microns employing a standardized imaging protocol (0.5 Al filter, 55kV, 180uA, 160ms exposure, 3 frame averaging, 0.7 degree rotation step). All raw data was reconstructed using Nrecon V1.6.9.4 with smoothing set to 1. No beam hardening or ring artifact correction was used. Slice data was assessed using the Skyscan software, DataViewer (Kontich, Belgium), as well as rendered and assessed in 3D using Drishti V2 Volume Exploration software (http://sf.anu.edu.au/Vizlab/drishti). For each mutant line assessed by microCT, a minimum of six affected males and six affected females were imaged and compared to a similar number of wildtype or unaffected background and sex-matched individuals.

PIXImus Densitometry

PIXImus scans (PIXImus, LUNAR, Madison, WI) which provide skeletal and body composition data such as Bone Mineral Density (aBMD, g/cm2), Bone Mineral Content (BMC,g), body mass (g), lean mass (g), fat mass (g), and % fat mass, are completed on groups of 6 male and 6 female 12 week old mutant and control mice. The skulls and bodies are scanned separately to provide independent data on skull aBMD and BMC and body aBMD and BMC. The PIXImus small animal densitometer (DEXA) has a resolution of 0.18×0.18 mm pixels and is equipped with software version 1.46. The PIXImus is calibrated routinely with a phantom utilizing known values, and a quality assurance test is performed daily. The variability in precision for measuring total body aBMD is, less than 1%, and approximately 1.5% for specialized regions such as the skull. The correlation between PIXImus aBMD measurements of 614 lumbar vertebrae compared to peripheral quantitative computerized tomography (pQCT) measurements was found to be significant ($p<0.001$; $r=.704$).

Statistical analysis

All data were analyzed with JMP11 Software for PC (SAS Institute Inc. Cary, NC) using a Tukey HSD test. Differences were considered different when p 0.05 Histograms were created with GraphPad Prism 6 Version 6.03 software for PC (GraphPad Software Inc. La Jolla, CA)

Supplementary Material

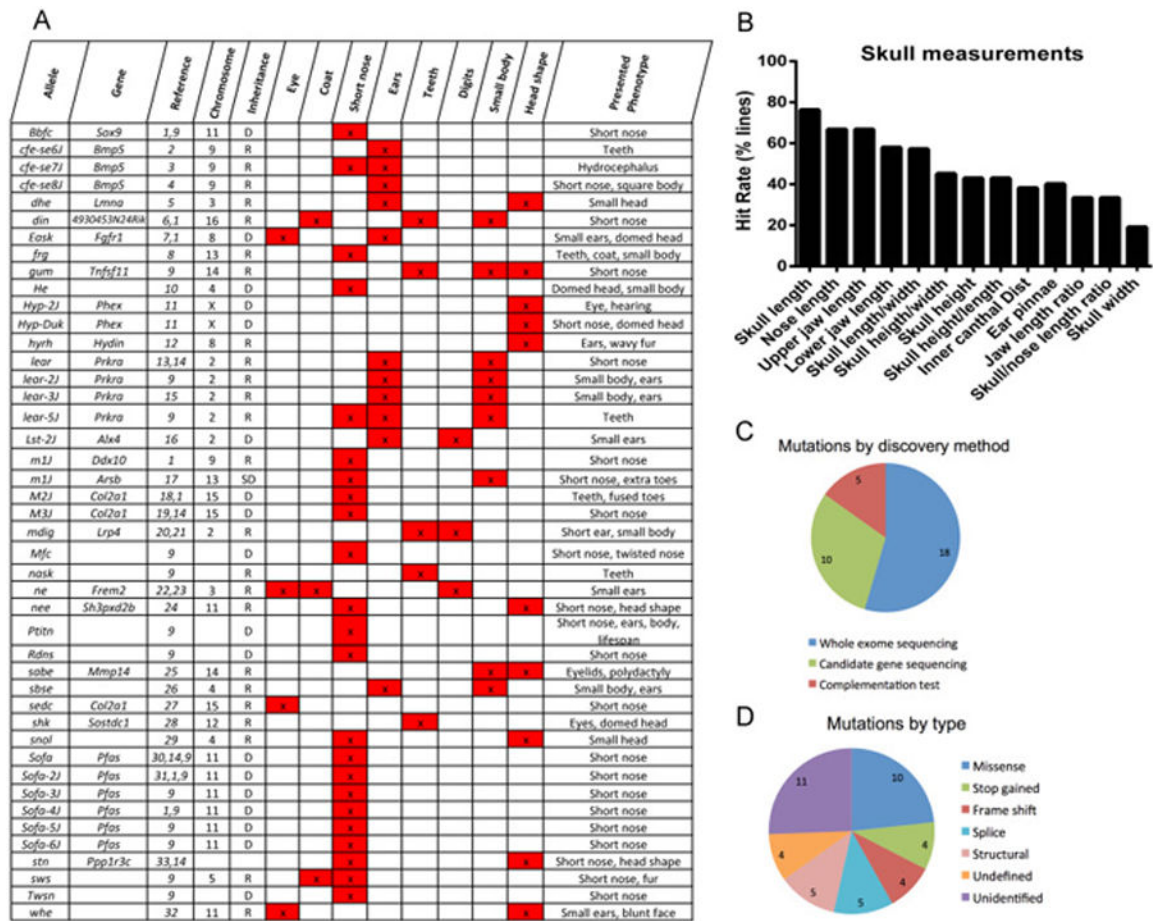Refer to Web version on PubMed Central for supplementary material.

Acknowledgments

References

Akiyama H, Chaboissier MC, Martin JF, Schedl A, Crombrugghe Bd. The transcription factor Sox9 has essential roles in successive steps of the chondrocyte differentiation pathway and is required for expression of Sox5 and Sox6. Genes & Development. 2002; 16:2813–2828. [PubMed: 12414734]

Ayadi A, Birling MC, Bottomley J, Bussell J, Fuchs H, Fray M, Gailus-Durner V, Greenaway S, Houghton R, Karp N, Leblanc S, Lengger C, Maier H, Mallon AM, Marschall S, Melvin D, Morgan H, Pavlovic G, Ryder E, Skarnes WC, Selloum M, Ramirez-Solis R, Sorg T, Teboul L, Vasseur L, Walling A, Weaver T, Wells S, White JK, Bradley A, Adams DJ, Steel KP, Hrabe de Angelis M, Brown SD, Herault Y. Mouse large-scale phenotyping initiatives: overview of the European Mouse Disease Clinic (EUMODIC) and of the Wellcome Trust Sanger Institute Mouse Genetics Project. Mamm Genome. 2012; 23:600–610. [PubMed: 22961258]

Bi W, Deng JM, Zhang Z, Behringer RR, de Crombrugghe B. Sox9 is required for cartilage formation. Nat Genet. 1999; 22:85–89. [PubMed: 10319868]

Bi W, Huang W, Whitworth DJ, Deng JM, Zhang S, Behringer RR, Crombrugghe Bd. Haploinsufficiency of Sox9 results in defective cartilage primordia and premature skeletal mineralization. Proceedings of the National Academy of Sciences of the United States of America. 2001; 98:6698–6703. [PubMed: 11371614]

Camargos S, Scholz S, Simon-Sanchez J, Paisan-Ruiz C, Lewis P, Hernandez D, Ding J, Gibbs JR, Cookson MR, Bras J, Guerreiro R, Oliveira CR, Lees A, Hardy J, Cardoso F, Singleton AB. DYT16, a novel young-onset dystonia-parkinsonism disorder: identification of a segregating mutation in the stress-response protein PRKRA. Lancet Neurol. 2008; 7:207–215. [PubMed: 18243799]

Curtain M, Donahue LR. A New Point Mutation in Col2a1 Causes a Shortened Nose and Cleft Palate. 2012

Curtain M, Heffner CS, Maddox DM, Gudis P, Donahue LR, Murray SA. A novel allele of Alx4 results in reduced Fgf10 expression and failure of eyelid fusion in mice. Mamm Genome. 2015; 26:173–180. [PubMed: 25673119]

Curtain M, Hurd J, Donahue LR. Stunted; A Short Face Mutation on Chromosome 19 in the Mouse. The Jackson Laboratory, Craniofacial Mutant Resource. 2008

Curtain MM, Dionne L, Fairfield HE, Donahue LR. A new, spontaneous short nose mutation in the mouse collagen type 2 alpha 1 gene. The Jackson Laboratory, Craniofacial Mutant Resource. 2014

Curtain MM, Donahue LR. Helicopter Ears: A Structural Mutation. The Jakson Laboratory, Craniofacial Mutant Resource. 2007a

Curtain MM, Donahue LR. A short face mutation on Chromosome 11. The Jackson Laboratory, Craniofacial Mutant Resource. 2007b

Curtain MM, Donahue LR. A mutation in the Arsb gene; a mouse model that resembles Mucopolysaccharidosis Type VI (MPS VI). The Jackson Laboratory, Craniofacial Mutant Resource. 2009

Curtain MM, Fairfield HE, Dionne L, Donahue LR. A new spontaneous short snout mutation in Pfas. The Jackson Laboratory, Craniofacial Mutant Resource. 2013

Curtain MM, Kane C, Donahue LR. An Ear Pinnae Mutation in the Mouse on Chromosome Two. The Jackson Laboratory, Craniofacial Mutant Resource. 2010

Dione L, Curtain M, Donahue LR. A Hydrocephalus Mutation with Rhinitis on Mouse Chromosome Eight. The Jackson Laboratory, Craniofacial Mutant Resource. 2008

Donahue LR, Chang B, Mohan S, Miyakoshi N, Wergedal JE, Baylink DJ, Hawes NL, Rosen CJ, Ward-Bailey P, Zheng QY, Bronson RT, Johnson KR, Davisson MT. A missense mutation in the

mouse Col2a1 gene causes spondyloepiphyseal dysplasia congenita, hearing loss, and retinoschisis. J Bone Miner Res. 2003; 18:1612–1621. [PubMed: 12968670]

Fairfield H, Gilbert G, Barter M, Corrigan R, Curtain M, Ding Y, D'Ascenzo M, Gerhardt D, He C, Huang W, Richmond T, Rowe L, Probst F, Bergstrom D, Murray S, Bult C, Richardson J, Kile B, Gut I, Hager J, Sigurdsson S, Mauceli E, Palma FD, Lindbald-Toh K, Cunningham M, Cox T, Justice M, Lowe MSS, Albert T, Donahue L, Jeddeloh J, Shendure J, Reinholdt L. Mutation discovery in mice by whole exome sequencing. Genome Biology. 2011a; 12

Fairfield H, Gilbert GJ, Barter M, Corrigan RR, Curtain M, Ding Y, D'Ascenzo M, Gerhardt DJ, He C, Huang W, Richmond T, Rowe L, Probst FJ, Bergstrom DE, Murray SA, Bult C, Richardson J, Kile BT, Gut I, Hager J, Sigurdsson S, Mauceli E, Palma FD, Lindblad-Toh K, Cunningham ML, Cox TC, Justice MJ, Spector MS, Lowe SW, Albert T, Donahue LR, Jeddeloh J, Shendure J, Reinholdt LG. Mutation discovery in mice by whole exome sequencing. Genome Biology. 2011b; 12:R86. [PubMed: 21917142]

Fairfield H, Srivastava A, Ananda G, Liu R, Kircher M, Lakshminarayana A, Harris BS, Karst SY, Dionne LA, Kane CC, Curtain M, Berry ML, Ward-Bailey PF, Greenstein I, Byers C, Czechanski A, Sharp J, Palmer K, Gudis P, Martin W, Tadenev A, Bogdanik L, Pratt CH, Chang B, Schroeder DG, Cox GA, Cliften P, Milbrandt J, Murray S, Burgess R, Bergstrom DE, Donahue LR, Hamamy H, Masri A, Santoni FA, Makrythanasis P, Antonarakis SE, Shendure J, Reinholdt LG. Exome sequencing reveals pathogenic mutations in 91 strains of mice with Mendelian disorders. Genome Research. 2015

Fuchs H, Gailus-Durner V, Neschen S, Adler T, Afonso LC, Aguilar-Pimentel JA, Becker L, Bohla A, Calzada-Wack J, Cohrs C, Dewert A, Fridrich B, Garrett L, Glasl L, Gotz A, Hans W, Holter SM, Horsch M, Hurt A, Janas E, Janik D, Kahle M, Kistler M, Klein-Rodewald T, Lengger C, Ludwig T, Maier H, Marschall S, Micklich K, Moller G, Naton B, Prehn C, Puk O, Racz I, Rass M, Rathkolb B, Rozman J, Scheerer M, Schiller E, Schrewe A, Steinkamp R, Stoger C, Sun M, Szymczak W, Treise I, Vargas Panesso IL, Vernaleken AM, Willershauser M, Wolff-Muscate A, Zeh R, Adamski J, Beckers J, Bekeredjian R, Busch DH, Eickelberg O, Favor J, Graw J, Hofler H, Hoschen C, Katus H, Klingenspor M, Klopstock T, Neff F, Ollert M, Schulz H, Stoger T, Wolf E, Wurst W, Yildirim AO, Zimmer A, Hrabe de Angelis M. Innovations in phenotyping of mouse models in the German Mouse Clinic. Mamm Genome. 2012; 23:611–622. [PubMed: 22926221]

Giggey J, Bauschatz J, Curtain M, Hurd J, Donahue LR. A cauliflower remutation to Bmp5. The Jackson Laboratory, Craniofacial Mutant Resource. 2007a

Giggey J, Curtain MM, Donahue LR. Sharkey, a new mutation in the Sostdc1 gene. The Jackson Laboratory, Craniofacial Mutant Resource. 2007d

Gorlin, RJ.; Stefan, LL. Syndromes of the Head and Neck. 3. Oxford University Press Inc.; New York: 1990.

Kane C, Curtain MM, Donahue LR. An ear pinna mutation in Fgfr1. The Jackson Laboratory, Crainiofacial Mutant Resource. 2012

Keane TM, Goodstadt L, Danecek P, White MA, Wong K, Yalcin B, Heger A, Agam A, Slater G, Goodson M, Furlotte NA, Eskin E, Nellaker C, Whitley H, Cleak J, Janowitz D, Hernandez-Pliego P, Edwards A, Belgard TG, Oliver PL, McIntyre RE, Bhomra A, Nicod J, Gan X, Yuan W, van der Weyden L, Steward CA, Bala S, Stalker J, Mott R, Durbin R, Jackson IJ, Czechanski A, Guerra-Assuncao JA, Donahue LR, Reinholdt LG, Payseur BA, Ponting CP, Birney E, Flint J, Adams DJ. Mouse genomic variation and its effect on phenotypes and gene regulation. Nature. 2011; 477:289–294. [PubMed: 21921910]

Keane TM, Wong K, Adams DJ, Flint J, Reymond A, Yalcin B. Identification of structural variation in mouse genomes. Front Genet. 2014; 5:192. [PubMed: 25071822]

Kist R, Schrewe H, Balling R, Scherer G. Conditional inactivation of Sox9: A mouse model for campomelic dysplasia. Genesis. 2002; 32:121–123. [PubMed: 11857796]

Kong YY, Yoshida H, Sarosi I, Tan HL, Timms E, Capparelli C, Morony S, Oliveira-dos-Santos AJ, Van G, Itie A, Khoo W, Wakeham A, Dunstan CR, Lacey DL, Mak TW, Boyle WJ, Penninger JM. OPGL is a key regulator of osteoclastogenesis, lymphocyte development and lymph-node organogenesis. Nature. 1999; 397:315–323. [PubMed: 9950424]

Lorenz-Depiereux B, Guido VE, Johnson KR, Zheng QY, Gagnon LH, Bauschatz JD, Davisson MT, Washburn LL, Donahue LR, Strom TM, Eicher EM. New intragenic deletions in the Phex gene

clarify X-linked hypophosphatemia-related abnormalities in mice. Mamm Genome. 2004; 15:151–161. [PubMed: 15029877]

Mao M, Thedens DR, Chang B, Harris BS, Zheng QY, Johnson KR, Donahue LR, Anderson MG. The podosomal-adaptor protein SH3PXD2B is essential for normal postnatal development. Mamm Genome. 2009; 20:462–475. [PubMed: 19669234]

Odgren PR, Pratt CH, Mackay CA, Mason-Savas A, Curtain M, Shopland L, Ichicki T, Sundberg JP, Donahue LR. Disheveled hair and ear (Dhe), a spontaneous mouse Lmna mutation modeling human laminopathies. PLoS One. 2010; 5:e9959. [PubMed: 20376364]

Orriss IR. The role of purinergic signalling in the musculoskeletal system. Auton Neurosci. 2015

Richtsmeier JT, Baxter LL, Reeves RH. Parallels of craniofacial maldevelopment in Down syndrome and Ts65Dn mice. Developmental Dynamics. 2000; 217:137–145. [PubMed: 10706138]

Robinson JT, Thorvaldsdottir H, Winckler W, Guttman M, Lander ES, Getz G, Mesirov JP. Integrative genomics viewer. Nat Biotechnol. 2011; 29:24–26. [PubMed: 21221095]

Seibler P, Djarmati A, Langpap B, Hagenah J, Schmidt A, Bruggemann N, Siebner H, Jabusch HC, Altenmuller E, Munchau A, Lohmann K, Klein C. A heterozygous frameshift mutation in PRKRA (DYT16) associated with generalised dystonia in a German patient. Lancet Neurol. 2008; 7:380–381. [PubMed: 18420150]

Seymour PA, Freude KK, Dubois CL, Shih HP, Patel NA, Sander M. A dosage-dependent requirement for Sox9 in pancreatic endocrine cell formation. Developmental Biology. 2008; 323:19–30. [PubMed: 18723011]

Simon-Chazottes D, Tutois S, Kuehn M, Evans M, Bourgade F, Cook S, Davisson MT, Guenet JL. Mutations in the gene encoding the low-density lipoprotein receptor LRP4 cause abnormal limb development in the mouse. Genomics. 2006; 87:673–677. [PubMed: 16517118]

Sweet HO, Marks SC Jr, MacKay CA, Johnson KR, Davisson MT. Dense incisors (din): a new mouse mutation on chromosome 16 affecting tooth eruption and body size. J Hered. 1996; 87:162–167. [PubMed: 8830097]

Ward-Bailey PF, Harris B, Donahue LR, Bronson R, Curtain M, Johnson K, Davisson M. Snubnose-like (snol), a new spontaneous skeletal mutation on Chromosome 4 in the mouse. The Jackson Laboratory, Craniofacial Mutant Resource. 2002

Zech M, Castrop F, Schormair B, Jochim A, Wieland T, Gross N, Lichtner P, Peters A, Gieger C, Meitinger T, Strom TM, Oexle K, Haslinger B, Winkelmann J. DYT16 revisited: exome sequencing identifies PRKRA mutations in a European dystonia family. Mov Disord. 2014; 29:1504–1510. [PubMed: 25142429]

Figure 1. A. Overall table of mutants characterized by the Craniofacial Mutant Resource.

Allele	Gene	Reference	Chromosome	Inheritance	Eye	Coat	Short nose	Ears	Teeth	Digits	Small body	Head shape	Presented Phenotype
Bbfc	Sox9	1,9	11	D			x						Short nose
cfe-se6J	BmpS	2	9	R				x					Teeth
cfe-se7J	BmpS	3	9	R			x	x					Hydrocephalus
cfe-se8J	BmpS	4	9	R				x					Short nose, square body
dhe	Lmna	5	3	R				x					Small head
din	4930453N24Rik	6,1	16	R	x	x	x		x		x		Short nose
Eosk	Fgfr1	7,1	8	D	x		x						Small ears, domed head
frg		8	13	R			x						Teeth, coat, small body
gum	Tnfsf11	9	14	R				x		x	x		Short nose
He		10	4	D			x						Domed head, small body
Hyp-2J	Phex	11	X	D								x	Eye, hearing
Hyp-Duk	Phex	11	X	D								x	Short nose, domed head
hyrh	Hydin	12	8	R									Ears, wavy fur
lear	Prkra	13,14	2	R				x			x		Short nose
lear-2J	Prkra	9	2	R				x			x		Small body, ears
lear-3J	Prkra	15	2	R				x			x		Small body, ears
lear-5J	Prkra	9	2	R			x	x			x		Teeth
Lst-2J	Alx4	16	2	D				x		x			Small ears
m1J	Ddx10	1	9	R			x						Short nose
m1J	Arsb	17	13	SD			x				x		Short nose, extra toes
M2J	Col2a1	18,1	15	D			x						Teeth, fused toes
M3J	Col2a1	19,14	15	D			x						Short nose
mdig	Lrp4	20,21	2	R				x	x				Short ear, small body
Mfc		9		D			x						Short nose, twisted nose
nask		9		R				x					Teeth
ne	Frem2	22,23	3	R	x	x			x				Small ears
nee	Sh3pxd2b	24	11	R			x					x	Short nose, head shape
Ptitn		9		D			x						Short nose, ears, body, lifespan
Rdns		9		D			x						Short nose
sobe	Mmp14	25	14	R							x	x	Eyelids, polydactyly
sbse		26	4	R				x			x		Small body, ears
sedc	Col2a1	27	15	R	x								Short nose
shk	Sostdc1	28	12	R				x					Eyes, domed head
snol		29	4	R			x					x	Small head
Sofa	Pfas	30,14,9	11	D			x						Short nose
Sofa-2J	Pfas	31,1,9	11	D			x						Short nose
Sofa-3J	Pfas	9	11	D			x						Short nose
Sofa-4J	Pfas	1,9	11	D			x						Short nose
Sofa-5J	Pfas	9	11	D			x						Short nose
Sofa-6J	Pfas	9	11	D			x						Short nose
stn	Ppp1r3c	33,14					x					x	Short nose, head shape
sws		9	5	R		x	x						Short nose, fur
Twsn		9		D			x						Short nose
whe		32	11	R	x							x	Small ears, blunt face

Figure 1. Identification and characterization of 43 spontaneous models of craniofacial dysmorphology

A. Overall table of mutants characterized by the Craniofacial Mutant Resource. A red "x" in each box indicates the model displays defects in this category. References cite the first description (often a web site description or direct Mouse Genome Informatics submission) of the mutant and the gene discovery. List is below. B. Overall hit rate for lines for each craniofacial measure as determined by caliper measurements on alizarin prepared skulls. A "hit" is called when a line displays a statistically significant (p<0.05) difference in any of the measures of the category. C. Segmentation of mode of discovery for the 33 mutations for which a gene has been identified. D. Distribution of types of mutations discovered, including unknown mutations ascertained by allelism tests and unidentified mutations in the resource.

References for Table A:

1: (Fairfield et al., 2015), 2: (Giggey et al., 2007a), 3: (Giggey et al., 2007a), 4: (Giggey et al., 2007a), 5: (Odgren et al., 2010), 6: (Sweet et al., 1996), 7: (Kane et al., 2012); 8: Marden 2007; 9: This study; 10: (Curtain and Donahue, 2007a); 11: (Lorenz-Depiereux et al., 2004); 12: (Dione et al., 2008); 13: (Curtain et al., 2010); 14: (Fairfield et al., 2011b); 15: Kane 2014; 16: (Curtain et al., 2015); 17: (Curtain and Donahue, 2009); 18: (Curtain and Donahue, 2012); 19: (Curtain et al., 2014); 20: (Simon-Chazottes et al., 2006) 21: Cook, 2003; 22: Curtain, 2008; 23: Karst; 2012; 24: (Mao et al., 2009); 25: Curtain, 2007; 26: Curtain, 2007; 27: (Donahue et al., 2003); 28: (Giggey et al., 2007d); 29: (Ward-Bailey et
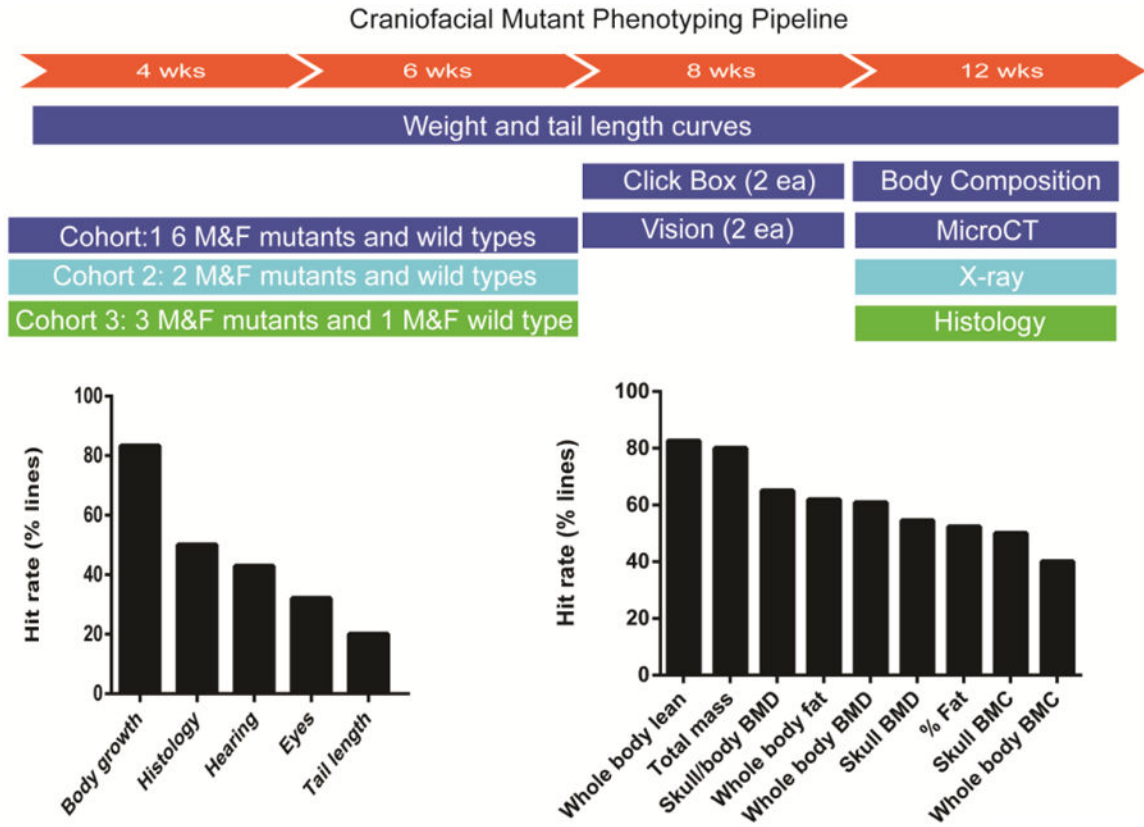
al., 2002); 30: (Curtain and Donahue, 2007b); 31: (Curtain et al., 2013); 32: Giggey, 2007; 33: (Curtain et al., 2008)

**Figure 2. Broad phenotyping pipeline reveals frequent pleiotropy in spontaneous craniofacial models**

A. Summary of the phenotyping tests performed arranged by age in weeks (orange bar at top). Mice are organized into three cohorts of 12, 4 and 6 mice respectively, split between both sexes. Weight and tail lengths are measured weekly for cohort 1, which are also assessed for hearing (click box) and vision (opthalmascope) defects. At the termination of the pipeline, mice are assessed for body composition by DEXA and heads are saved for microCT scanning. Cohort 2 is X-rayed at 12 weeks of age, and Cohort 3 is reserved for a standardized pathology screen. B. Overall hit rate for lines within each phenotyping category. A "hit" is called when a line displays a statistically significant (p<0.05) difference in any of the measures of the category. C. Further segmentation of the body growth and composition category showing a high hit rate for whole body lean and total mass.
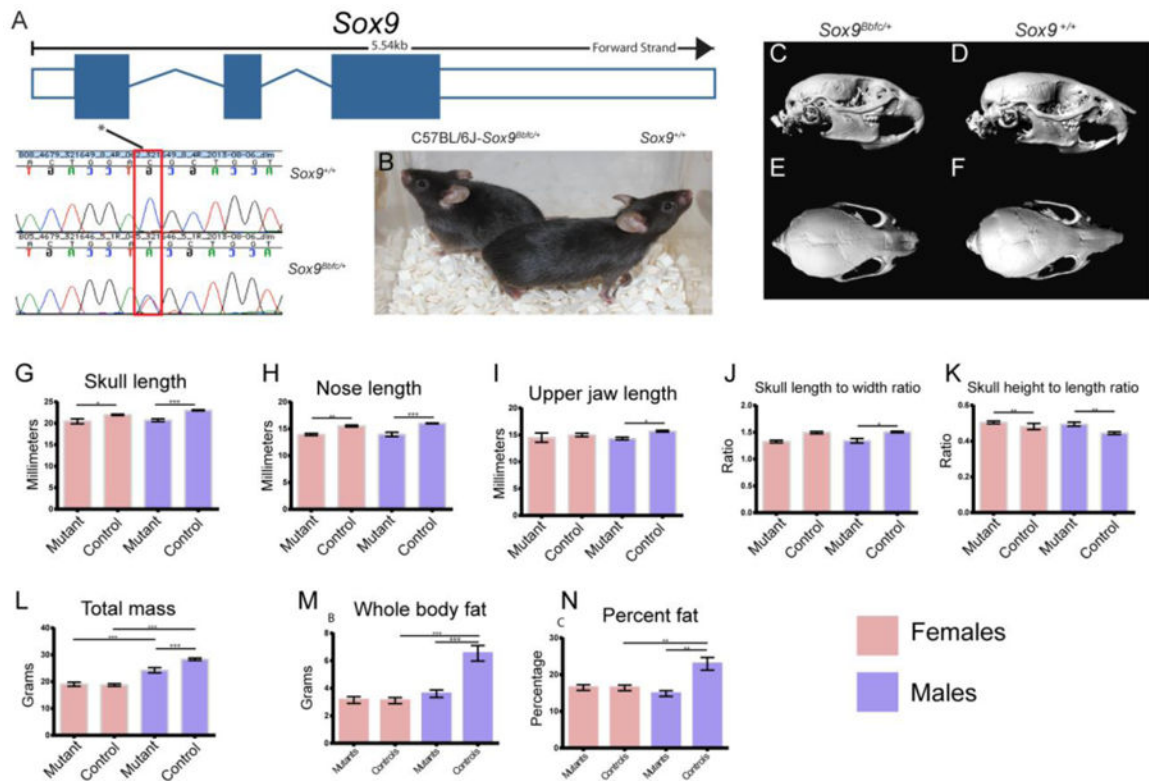
Figure 3. Identification and characterization of Babyface (*Bbfc*), a viable allele of *Sox9*

A. Schematic of the Sox9 allele structure and positioning of the Bbfc mutation in exon 1. The chromatogram shows C to T transition which results in a missense T87M mutation. C-F. 3D surface renderings of microCT images of Bbfc mutant (C,E) and control (D, F) heads at 12 weeks of age revealing the shorter, domed appearance of the skull. Quantitation of skull dimensions shows significant reduction in total skull length (G) and nose length (H) in mutants for both sexes and reduction in upper jaw length (I) for males only. The ration of skull length to width was lower in mutant males (J) only, but both sexes displayed a significant increase in the skull height to length ratio (K). Body composition measures showed sexually dimorphic differences in total mass (L), whole body fat (M) and percentage fat (N), where only males showed a difference between mutants and controls. Normal sexual dimorphism between controls is seen in all three measures. For all comparisons, a line connects significantly different measures, with p values indicated by the asterisk: * = p <0.05, ** = p<0.01, *** = p<0.0001.
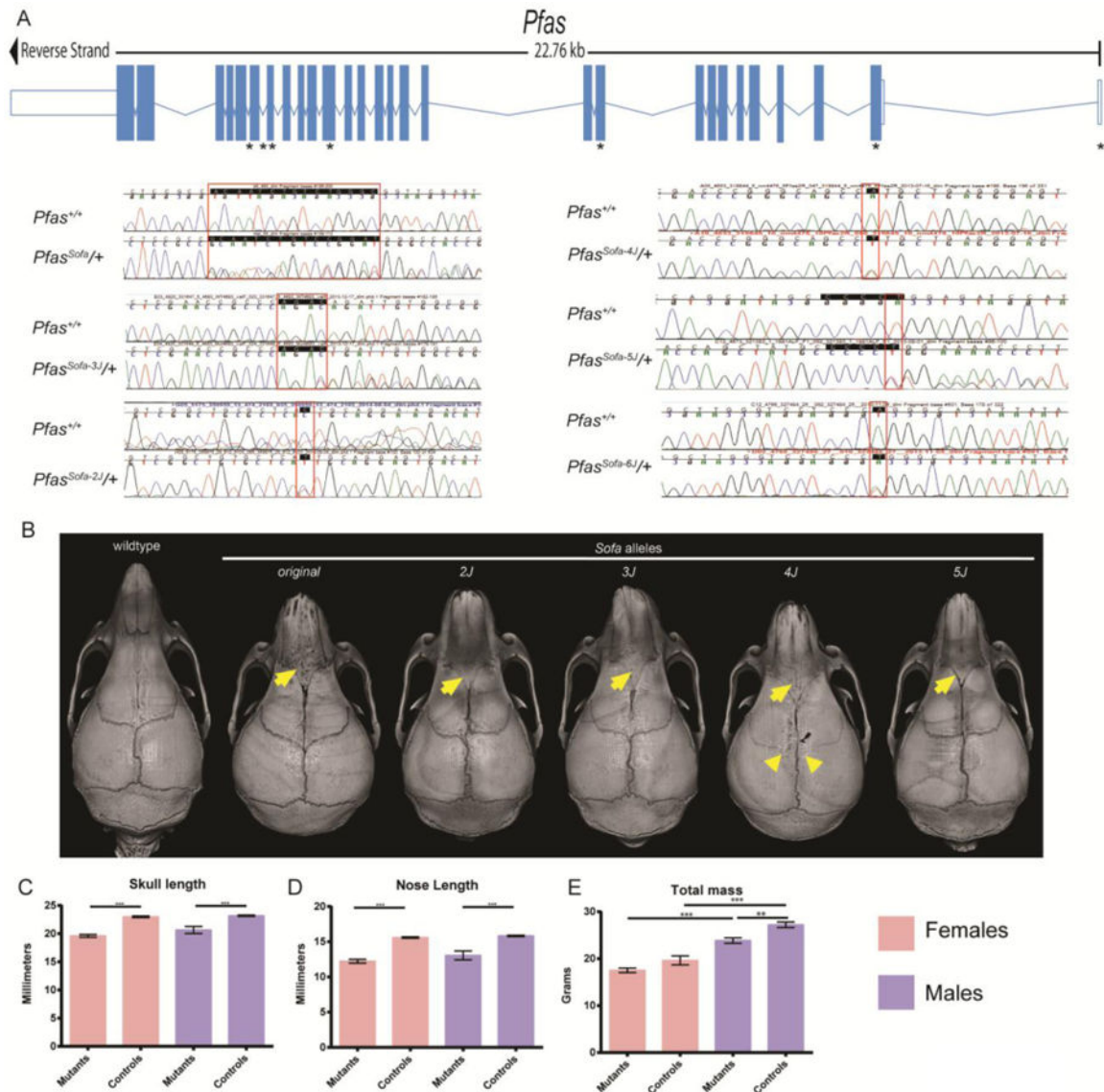
Figure 4. Allelic series of the gene *Pfas* reveals a role in craniofacial development
A. Schematic of the Pfas gene structure and positioning of the various Sofa mutations, and chromatograms below show validation of the mutation structure *Sofa*: 15bp deletion in exon 7, Sofa-2J: C to T transition at the intron 6/exon 7 splice site (11: 68,814,092), Sofa3J: 4 bp deletion in exon 27 (11:68801981-68801984), Sofa-4J: an A to T transversion in exon 19 (11:68,805,396), Sofa-5J: a single C insertion in exon 28 (11:68,801,643), and Sofa-6J: an A to T transversion in exon 11 (11:68,998,030). All coordinates are GRCm38/mm10. B. Dorsal views of rendered microCT scans of a wildtype (left) and one affected individual from five of the distinct *Sofa* alleles: *Sofa, Sofa-2J, Sofa-3J, Sofa-4J* and *Sofa-5J*. The cranioskeletal changes seen in all lines include a shortened cranial length and domed skull with marked midfacial deficiency. A diamond-shaped interfrontal bone that prematurely fuses with the nasal bones (yellow arrows) is a consistent feature of the *Sofa* allelic series. Measurements of Sofa skulls showed a significant reduction in skull length (C) and nose length (D), and mutants are typically smaller (E). For all comparisons, a line connects
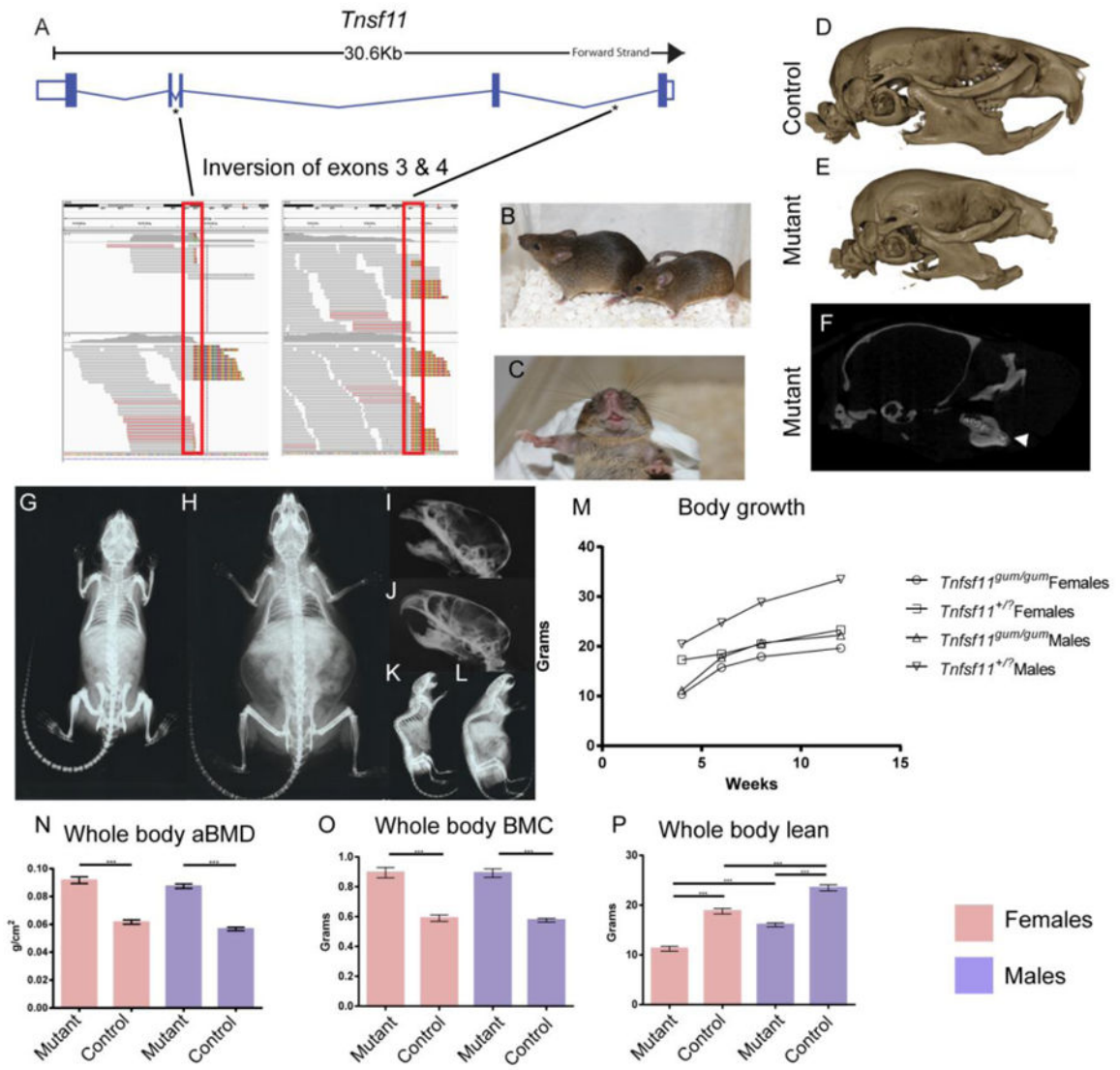
significantly different measures, with p values indicated by the asterisk: ** = $p<0.01$, *** = $p<0.0001$.

Figure 5. Failure of tooth eruption and osteopetrosis in the spontaneous mutation gummy (gum) is caused by a novel inversion in *Tnfsf11*

A. Schematic of the Tnfsf11 gene with inversion interval marked by asterisks. Linked are screenshots from IGV viewer showing the mismatch signature of the assembled reads (multi-colored horizontal bars with multiple colors). Grey aligned reads outlined in red indicate the paired read is unmapped because they are hybrid reads over the inversion breakpoint. The inversion thus disrupts the Tnfsf11 gene after exon 2, although it is strictly possible internal revealed splice acceptors or splicing to exon 5 could occur, but this was not tested. B, C. Images of gum mice (right in B) showing small size and failure of tooth eruption in C. D-E. 3D surface rendering of microCT images of mutant (D) and control (E) mice showing reduced size and high degree of thickening overall. The mandible is hypoplastic, the angle and condyle of the mandible is misshapen and the maxillary-premaxillary suture is missing. A sagittal cross section of the 3D stack shows present, but unerupted, molars and an ectopic tooth in the diastema (F). X-rays of mutants (G, I, K) show dramatically denser bones and completely filled medullary space in the long bones versus

controls (H, J, L). Both male and female affected mice are growth retarded (M), showing reduced weight increase between 4 and 12 weeks of age. Whole body bone mineral density (BMD) is significantly higher in both males and females (N), while skull BMC (O) and skull to body BMD ratio are less in mutants, owing to the reduced head size. For all comparisons, a line connects significantly different measures, with p values indicated by the asterisk: * = p <0.05, **p<0.01, ***p<0.0001.
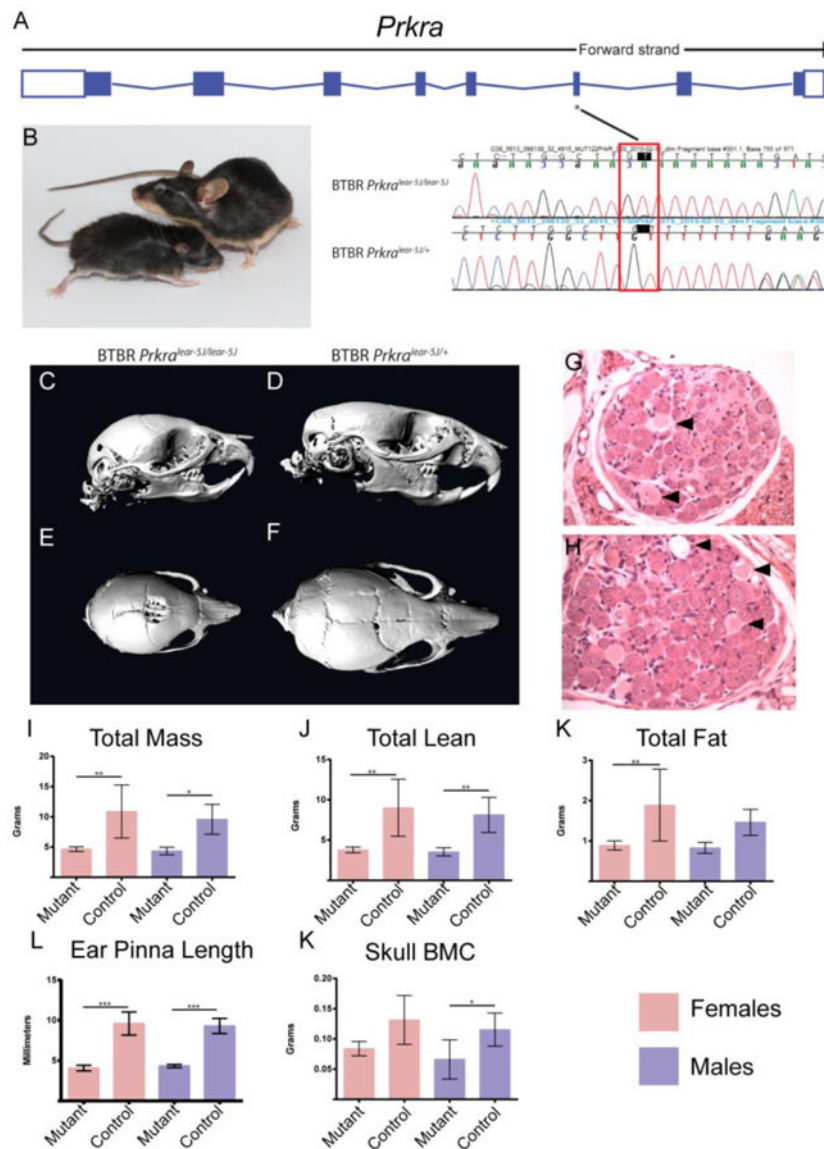
Figure 6. Remutation of the gene *Prkra* (*lear5J*) on the BTBR T[+] Itpr3[tf]/J genetic background is a model for human Dystonia 16

A. Schematic of the Prkra gene showing the location of the mutation in exon 3. Subsequent validation of the G to GT insertion is shown in the chromatogram, which results in a frame shift and a premature stop. B. Image of affected mouse with littermate control showing the dramatically reduced body size. Note the distinctive coat color of the BTBR T[+] Itpr3[tf]/J strain. C. Three dimensional surface renderings of microCT images showing the shorter and misshapen skull in mutants (C, E) versus controls (D, F). Incomplete ossification and an open foramen is seen in mutant skulls (E). G. Ganglion with dead or dying neurons from a three-week-old mutant mouse. Most neurons contain bright red cytoplasm while the cytoplasm is paler in dying ones. Top arrow indicates a space where the neuron has died. H: A second ganglion typical of mutant with arrows indicating dying neurons. Controls had normal ganglia (not shown). Significant differences for total mass and total lean (I,J) are seen for both sexes. Ear pinna length (L), consistent with the *lear* phenotype, were smaller in

mutants of both sexes as well. Females only showed a significant reduction in total fat (K), while males only showed a reduction in skull BMC (K), although females trended lower as well. For all comparisons, a line connects significantly different measures, with p values indicated by the asterisk: * = p <0.05, **p<0.01, ***p<0.0001.